Polymer 226 (2021) 123787

Contents lists available at ScienceDirect

Polymer

journal homepage: www.elsevier.com/locate/polymer

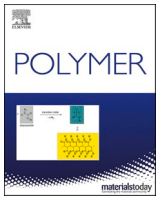

Epoxy-based composites reinforced with imidazolium ionic liquid-treated aramid pulp

Eduardo Fischer Kerche [a,*], Vinícius Demétrio da Silva [b], Eduardo Fonseca [a], Nicholas Alves Salles [a], Henri Stephan Schrekker [b], Sandro Campos Amico [a]

[a] PPGE3M, Federal University of Rio Grande do Sul – UFRGS, Av. Bento Gonçalves 9500, Porto Alegre, RS, 91501-970, Brazil
[b] Laboratory of Technological Processes and Catalysis, Federal University of Rio Grande do Sul – UFRGS, Av. Bento Gonçalves 9500, Porto Alegre, RS, 91501-970, Brazil

ARTICLE INFO

Keywords:
Imidazolium ionic liquids
Composites
DGEBA/TETA epoxy
Surface treatment
Polyaramid pulp
Toughness agent

ABSTRACT

Two types of physisorbed imidazolium ionic liquids (IL), 1-*n*-butyl-3-methylimidazolium chloride (**C_4MImCl**) or 1-*n*-butyl-3-methylimidazolium acetate (**C_4MImAc**), were used for the surface treatment of polyaramid pulp (AP), aiming to enhance the interaction with an epoxy matrix. The treatments promoted a greater defibrillation of AP, which was most likely due to an interference of IL in the hydrogen bonding network of polyaramid. Composites of AP/epoxy (0.2, 0.4 or 0.6 parts per hundred of resin (phr)) were prepared, and those with 0.4 phr of IL-treated AP presented enhanced mechanical properties, compared to the neat or the untreated AP composites. Better homogeneity and stronger bonding between AP and the epoxy matrix were also observed, especially in the case of AP treated with **C_4MImCl**. Moreover, the AP surface treatment increased the glass transition temperature and the storage moduli in both glassy and rubbery regions. The fracture toughness improvement of the composites was also achieved with the addition of the IL-treated AP.

1. Introduction

The most common epoxy resin for advanced composites is based on diglycidyl ether of bisphenol A (DGEBA), with low viscosity before curing, and high mechanical properties and thermal stability. Its brittle character may be decreased by adding a second phase, e.g., inorganic/rigid [1,2] or rubbery [3] micro- or nano-particles [4,5], thermoplastics [6] and hyperbranched polymers, or even by increasing the chain length between crosslinks [7]. However, some of these strategies promote a negative effect on the performance of the epoxy resin or its composite, such as reduction in stiffness, strength, or glass transition temperature (T_g).

Short- or micro-fibers can also be added to enhance impact strength and energy absorption of polymers [8], and present advantages over long fibers associated with mass production of complex shaped parts with low fiber content [9]. Organic aramid fibers, including those from poly-p-phenylene terephthalamide (PPTA), present some advantages compared to the inorganic ones, such as lower density and greater capacity to absorb impact energy, which in turn potentialize increments in composite toughness [10]. Moreover, AP is a tough and fibrillated reinforcement, used in many types of resin-based composites, aiming to improve the wear resistance to fabricate materials for friction applications [11].

PPTA reinforcement has been used in epoxy matrix, focusing mainly on increasing the interlaminate properties of laminates [12,13]. Despite the gains, the studies report that the dispersion of PPTA into epoxy is still a challenge. Dispersion of an aramid pulp (AP) may be assisted by acetone, but this impacts the mechanical properties of the resin since solvent evaporation during resin curing leads to bubble entrapment. Thus, new techniques for the dispersion of PPTA into epoxy resin and/or the use of compatibilizers are still demanded.

Several strategies are reported for the surface modification of AP. Some of them include chemical grafting (e.g., acid/base assisted grafting, fluorination), physical methods (e.g., plasma, γ-ray irradiation, ultraviolet initiation), coating methods (e.g., using rubber, epoxy, polyethylene glycol) and by the deposition of nanostructures (e.g., nano particles, rods and sheets) [14]. Despite the greater compatibility of the aramid with the polymer matrix, some of the cited techniques are expensive and/or cause a great physical demerge to the aramid, which can consequently decrease the mechanical properties of the produced

* Corresponding author.
E-mail address: eduardo.kerche@ufrgs.br (E.F. Kerche).

https://doi.org/10.1016/j.polymer.2021.123787
Received 2 March 2021; Received in revised form 10 April 2021; Accepted 16 April 2021
Available online 28 April 2021

composite.

Physiosorbed imidazolium ionic liquids (IL) may be used to improve the interfacial characteristics of PPTA and, in turn, the dispersion of the fiber into the prepolymer matrix. For instance, 1-*n*-butyl-3-methylimidazolium chloride (**C_4MImCl**), 1-n-butyl-3-methylimidazolium methanesulfonate (**C_4MImMeS**), 1-carboxymethyl-3-methylimidazolium chloride (**HO_2CC_1MImCl**), 1-triethyleneglycol monomethyl ether-3-methylimidazolium methanesulfonate (**C_7O_3MImMeS**) (Fig. 1) have been used to treat aramid for the preparation of styrene-butadiene rubber (SBR) [15,16], hydrogenated nitrile butadiene rubber (HNBR) [17], laminated epoxy-based composites [18] and also for bio-based rigid polyurethane foams [19]. Due to the contribution of the imidazolium cation π-cloud in π–π interactions and their hydrogen atoms (C_2–H, C_4–H, and C_5–H) in hydrogen bonds with adjacent polymer matrix chains, these IL were considered promising compatibilizers. Disruption of the hydrogen bonding network within the aramid fibers due to the IL anion may cause fibrillation, resulting in easier mechanical anchoring of the polymer matrix in the fibrils, favoring their role as compatibilizers [20,21].

Despite the reported works on the use of AP to enhance the performance of composites, it is hard to find reports on the chemical modification of AP surface, especially with physiosorbed IL and its use into epoxy-based composites. Hence, the objective of this work was to investigate the effect of two types of IL on the surface modification of AP, focusing on the chemical and physical interactions with the polymer matrix and the related changes in mechanical, viscoelastic and toughness properties of the final composites.

2. Experimental

The reagents used in this study were DGEBA GY-260 Araldite® resin and triethylenetetramine (TETA) hardener AH-260 purchased from Huntsman Co. (São Paulo, Brazil). The IL **C_4MImCl** and **C_4MImAc** (Fig. 1) were used as purchased from Sigma-Aldrich (St. Louis, USA). The NMR spectra of each IL and IL-TETA mixtures were recorded in a Bruker (400 MHz) equipment, model Avance I at room temperature. The chemical shifts are given in ppm and referenced to the residual solvent signal (DMSO-d_6 = 2.50 (^{1}H)). Aramid pulps were kindly donated by Dupont® and, according the manufacturer, the pulps present the length of 0.5–1 mm and bulk density of 48–160 kg m^{-3} [22].

2.1. AP treatment and characterization

Treatment of the AP was performed in an ethanolic solution with 5 wt% of IL in relation to the AP mass, and followed previous reports [15–18]. The AP-IL mixture was placed in an ultrasonic bath at 50 °C for 30 min, left to evaporate the solvent for 24 h at room temperature and then placed in a vacuum oven for 12 h at 110 °C. The effectiveness of the treatment was assessed using scanning electron microscopy (SEM), thermal gravimetric analysis (TGA) and Fourier transform infrared spectroscopy (FTIR). A TA Instruments Q50 thermogravimetric analyzer (New Castle, EUA) was used to determine the IL-content adsorbed on the AP. A single analysis was performed for each treatment, with ca. 10 mg of sample and heating at 20 °C/min, from 35 to 800 °C in N_2 atmosphere. FTIR in the mid-infrared range (4000-500 cm^{-1}) was performed in a Spectrum 1000 spectrometer from Perkin Elmer. The surface of the commercial AP and the IL-treated AP were analyzed using a Phenom ProX Desktop microscope, with an acceleration of 15 kV.

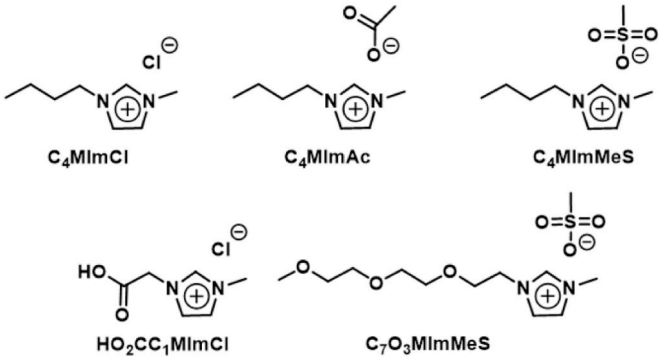

Fig. 1. Chemical structures of the IL previously studied as compatibilizers in aramid pulp reinforced composites (**C_4MImCl**, **C_4MImMeS**, **HO_2CC_1MImCl** and **C_7O_3MImMeS)** [15–19] and the ones explored in this study (**C_4MImCl**, **C_4MImAc**).

2.2. Epoxy composites preparation and characterization

The commercial AP or IL-treated AP were added to the epoxy resin followed by 5 min of mechanical stirring. This mixture was placed in an ultrasonic bath for 20 min at 50–60 Hz. The TETA hardener (13.0 phr) was added and the mixture was again mechanically stirred for 5 min, followed by another ultrasonication for 20 min at 50–60 Hz. After that, the mixture was placed into a degasser for 10 min under negative pressure to remove bubbles, and then the mixture was poured into silicone molds and cured at room temperature for 24 h. Subsequently, the specimens went through a post-curing process in an oven at 60 °C for 12 h. The adopted nomenclature uses **E** for epoxy, **AP** for aramid pulp, **.Cl** for **C_4MImCl** treated AP, **.Ac** for **C_4MImAc** treated AP, and the numbers **2, 4** and **6** for, respectively, 0.2, 0.4 and 0.6 parts per hundred of AP in relation to the resin (phr).

Differential scanning calorimetry (DSC) was performed for uncured composites in a DSC Q20 from TA Instruments in the temperature range of 25–200 °C at a heating rate of 10 °C/min, for freshly prepared epoxy and AP composites. The evaluated thermodynamic parameters were the onset temperature (T_{onset}), maximum curing rate temperature (T_{peak}) and total heat of reaction (ΔH), this latter calculated by the integration of the exothermic peak.

Three-point bending tests of neat epoxy and those with incorporated AP were performed using 70 × 12.7 × 3.0 mm specimens following the ASTM D790–17 standard to obtain flexural strength (σ_f) and flexural modulus (E_f). Fracture toughness was assessed according to the ASTM D5045-14 standard, using single-edge notch bending (SENB) specimens with 75 × 10 × 5 mm dimensions. The notch was made with a Ceast NotchVis V-notch machine in the middle of the specimen's length, and a pre-crack was made until half the width by carefully sliding a sharp razorblade. After testing, the cracked sample surface was analyzed via optical microscopy prior to the calculation of the critical stress intensity factor (K_{IC}) (Eq. (1)) and the critical strain energy release rate (G_{IC}) (Eq. (2)). The length of the zone of plastic deformation (ZPD) was measured using SEM images, with the same equipment and methodology described above. At least three samples were tested to validate the results.

$$K_{IC} = \left(\frac{P_Q}{WB^{1/2}}\right) f(x) \quad (1)$$

$$G_{IC} = \frac{U}{(WB\phi)} \quad (2)$$

Where: P_Q is the maximum supported load by the sample; W and B are the sample's width and depth, respectively; f(x) is a function that depends on the crack geometry after testing; U is the energy generated by the applied strain, obtained by integrating the curve of load *vs.* displacement, and ϕ is a factor to calibrate the measurements.

Inferential statistical analysis was performed on the obtained mechanical properties, using as factors the wt.% of reinforcement and the IL used to treat the AP. Normality and homogeneity of each level were verified by Shapiro-Wilk and Levane tests, respectively. After that, one-way ANOVA and averaging tests were performed following the LSD

Fischer procedure with 95% confidence.

Dynamical mechanical analyses (DMA) were performed in prismatic specimens (dimensions: 17.5 × 12.7 × 3.0 mm) under single cantilever clamp, in a TA Instruments DMA 2980 equipment, at a frequency of 1.0 Hz, from 30 to 200 °C. The T_g was determined from the tan delta peak. To evaluate the influence of the content of AP used, as well as the influence of IL treatment, the effectiveness of filler reinforcement constant, C, was calculated, as suggested by Ornaghi et al. (2010) [8], following Eq. (3):

$$C = \left(\frac{(E'_g / E'_r)_{Composite}}{(E'_g / E'_r)_{Resin}}\right) \quad (3)$$

Where: E'_g and E'_r are the storage moduli related to the glassy and rubbery regions, respectively.

3. Results and discussion

3.1. Aramid pulp surface treatment

Fig. 2 shows the TGA results for neat AP, the IL **C_4MImCl** and **C_4MImAc**, and both IL-treated AP. The weight percentage of IL in the treated AP was determined considering the maximum mass loss for each IL decomposition (i.e., the temperature for the maximum DTG peak), which corresponds to 293 °C and 260 °C for **C_4MImCl** and **C_4MImAc**, respectively. The contents of **C_4MImCl** and **C_4MImAc**, assessed by this methodology were, respectively, 3.5 wt% and 2.0 wt% in relation to the AP mass. These results perhaps are related to the losses of IL during the AP treatment or a heterogeneous IL distribution within the AP.

The FTIR spectra (Fig. 3) displays the characteristic peaks of each material in accordance with the literature [15–17]. Both untreated and the two IL-treated AP presented three characteristic aramid peaks, at 3320 cm^{-1} (NH stretching vibrations in a secondary amide in trans form

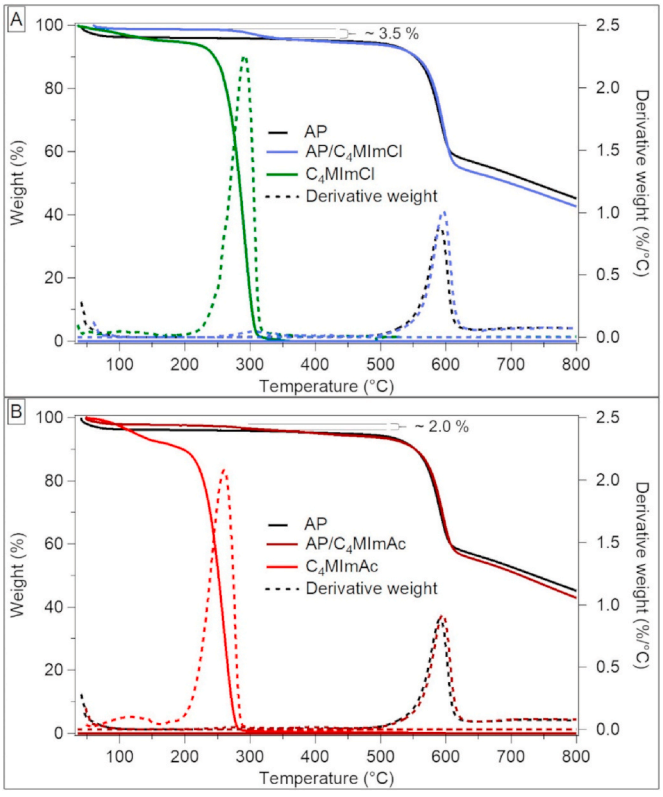

Fig. 2. TG and DTG curves of AP, **C_4MImCl** and AP/**C_4MImCl** (A), and AP, **C_4MImAc** and AP/**C_4MImAc** (B).

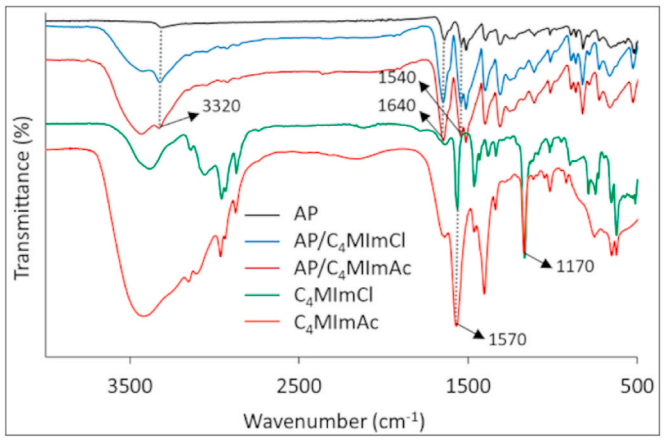

Fig. 3. FTIR transmittance spectra of **AP**, **C_4MImCl**, **C_4MImAc**, **AP/C_4MImCl** and **AP/C_4MImAc**.

with a bonded hydrogen), 1640 cm^{-1} (CO amide stretching for hydrogen-bonded amide groups) and 1540 cm^{-1} (NH group) [11,23]. Regarding the IL, for both, a characteristic broad peak in the 3330–3450 cm^{-1} range can be seen, probably related to the O–H from water, formed during the analysis [17]. For **C_4MImAc** and **C_4MImCl**, the peaks at 1570–1164 cm^{-1} can be attributed to the imidazolium ring stretching modes. The peak at 1170 cm^{-1} for **C_4MImAc** can be attributed to the C═O bond stretching [24,25]. In the FTIR spectra, it is not possible to identify the IL related peaks in the treated fibers, perhaps since most of it was absorbed by AP and are located inside the pulp, leaving only a small part on its outer surface.

Fig. 4 presents some images of AP when treated with different types of IL. In Fig. 4a is possible to see that the pulps present a smooth and regular surface with short and fibrillated characteristics, as reported by the manufacturer. This characteristic can be an issue for the manufacturing of composite materials, since the anchoring and physical interactions with the matrix is reduced. When AP was treated with **C_4MImCl** (Fig. 4b) or **C_4MImAc** (Fig. 4c), the fiber became much more fibrillated and its surface rougher and more irregular. The attack of the IL on the AP was probably related to the formation of new hydrogen bonds and π-stacking interactions in the IL-AP system. This would break pre-existing hydrogen bonds and π-stacking interactions among adjacent aramid chains [20]. Moreover, when these pulps (treated with 5 wt% of IL) are compared with those treated with lower amount of IL (0.5; 1.0 and 2.0 wt%) the higher defibrillation and rougher surface is evident [15–19]. The AP defibrillation can have beneficial effects related to the increase in mechanical anchoring between AP and the matrix; and a more fibrillated system also has greater surface area, which favors overall adhesion. However, when the IL treatment is compared with other AP surface treatments (e.g., metalation, bromination, grafting [26] and plasma [27]), it is clear the lower aggressiveness of the process.

The hydrogen bond formation between the IL and the triethylenetetramine (TETA) based AH-260 hardener was studied by ^{1}H NMR spectroscopy, and the spectra of **C_4MImCl**, **C_4MImCl** + AH 260 (Fig. S1), **C_4MImAc** and **C_4MImAc** + AH 260 (Fig. S2) confirmed these interactions. According to literature, when the donor-acceptor distance decreases, as a result of stronger hydrogen bonding, ^{1}H shielding becomes smaller. Thus, the signals of the peaks related to the imidazolium ring hydrogens (C_2–H, C_4–H, C_5–H) shifted to higher frequencies. This larger proton de-shielding may be associated with a hydrogen bond strengthening [28,29]. When **C_4MImCl** or **C_4MImAc** was in the presence of the hardener, the peaks related to the imidazolium ring hydrogens (C_2–H, C_4–H, C_5–H) shifted. For the most acidic hydrogen (C_2–H), the greater displacement is observed, from 9.57 ppm to 9.84 ppm for the **C_4MImCl** + AH 260 mixture, and from 10.31 to 10.41 for the **C_4MImAc** + AH 260 mixture.

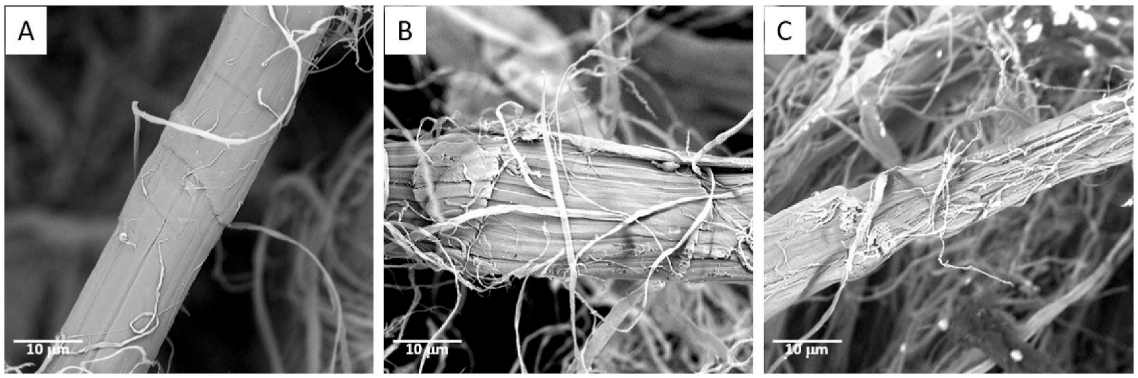

Fig. 4. SEM micrographs of: (A) commercial AP, (B) AP treated with 5 wt% of **C_4MImCl** and (C) AP treated with 5 wt% of **C_4MImAc**.

3.2. Treated aramid pulp/epoxy composites' properties

3.2.1. Curing kinetic

Figure S3 shows the DSC curve for the curing kinetic of the samples. All samples presented an exothermic peak during curing, indicating the formation of a high crosslinking density, as expected. Moreover, according McCoy et al. [30], the curing kinetic of a DGEBA epoxy resin is a complex reaction system and the use of fillers may promote different events in the DSC curve shape [31]. Table 1 summarizes the main temperatures related to the curing of the epoxy and epoxy IL-treated AP composites. No significant differences on T_{onset} and T_{peak} are presented for all composites or neat epoxy, which means that AP does not influence on the beginning of epoxy curing [31]. On the other hand, the heat realized (ΔH) during the cure presents a slight increment, when AP is used, which may be attributed to the catalytic effect of AP in the ring opening reaction of epoxy, by the presence of amine groups on the AP surface [32].

3.2.2. Viscoelastic characteristics

Fig. 5 shows the storage modulus curves for the studied cases. All samples presented three main regions observed for thermoset polymers, i.e., glassy (about 30–80 °C), rubbery (above 120 °C) and glass transition between them. For a clearer analysis of the AP effect in reinforcing epoxy, a normalized modulus was calculated for both glassy (at 40 °C) and rubbery (at 140 °C) regions (i.e., the ratio between storage modulus of the composite, E_c, and that of neat epoxy, E_m) (Table 2). Comparing those composites reinforced with untreated and AP treated with **C_4MImCl**, there were an increment on E' for all contents evaluated, in both glassy and rubbery regions. For the glassy region, the discussion follows for the three-point bending tests.

However, when the normalized moduli is evaluated for the rubbery region, the balance of the optimized content of 0.4 phr for those E/AP was able to equal the results for those E/AP6.Cl. Despite the higher affinity of those treated AP with epoxy matrix, the content of the filler for the rubbery region is more important for the load transferring through the composite's components, a result also related to the values for constant C. Those composites with 0.4 phr of untreated AP presented the lower values for C constant. According Ornaghi et al. [8], the lower the C constant, the higher the effectiveness of the filler to reinforce the composite matrix and the maximum effectiveness to transfer stresses between fiber and matrix takes place. In other words, the AP content will

Table 1
Summarized DSC results for the curing kinetic of the samples.

Sample	T_{onset} (°C)	T_{peak} (°C)	ΔH (J/g)
E	56.4	97.6	281.5
E/AP4	57.7	101.8	331.0
E/AP4.Cl	59.4	99.8	326.2
E/AP4.Ac	55.3	102.2	294.8

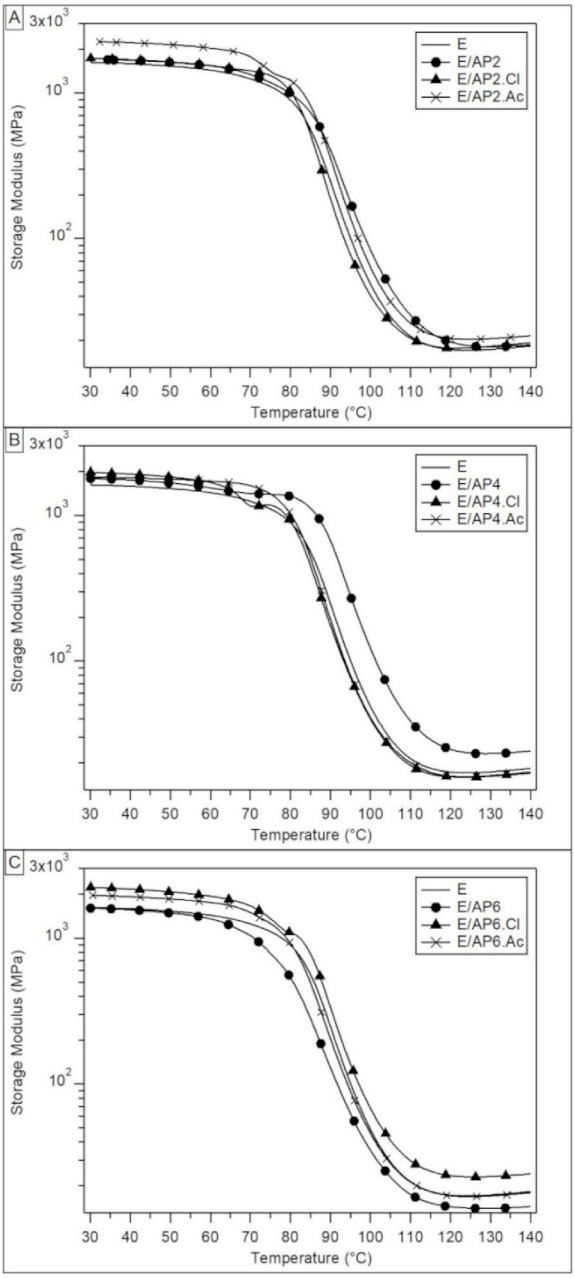

Fig. 5. Storage modulus curves for epoxy and the epoxy composites with 0.2 phr (A), 0.4 phr (B) and 0.6 phr (C) of AP.

Table 2
Normalized storage moduli and effectiveness of fillers reinforcement (C) for the studied epoxy/AP composites.

Sample	E_c/E_m (at 40 °C)	E_c/E_m (at 140 °C)	C (40/140 °C)
E/AP2	1.05	1.02	1.03
E/AP4	1.10	1.32	0.83
E/AP6	0.98	0.79	1.24
E/AP2.Cl	1.06	1.06	1.01
E/AP4.Cl	1.21	0.93	1.30
E/AP6.Cl	1.36	1.32	1.03
E/AP2.Ac	1.39	1.18	1.18
E/AP4.Ac	1.14	0.95	1.20
E/AP6.Ac	1.21	0.98	1.23

play a major role, compared to the treatment, for the transference of relaxation times through the composite's components (i.e., between the epoxy matrix and AP).

The loss modulus curves for all samples are presented in Fig. 6. For epoxy reinforced with 0.2 phr of AP (Fig. 6a), a peak close to 75 °C is seen for the AP treated with **C_4MImAc**, related to a β transition, i.e., relaxation of the AP phase. Because the loss modulus of aramid is four orders of magnitude lower than its storage modulus [10], relaxation of the aramid chains occurs at lower temperature. The same trend is illustrated in Fig. 6c for the systems filled with 0.6 phr of AP, regardless of the treatment. The shoulder seen for these systems emphasizes the hypothesis that the filler content plays a more significant effect on the homogenous relaxation of the composite (i.e., when there is only a single peak in the E" curve) than the IL treatment. In other words, 0.6 phr of AP promotes two relaxations for the composites, the first one related to AP and the second to the epoxy matrix, which can be related to a higher number of aggregates formed for this content.

The better bonding between AP and epoxy promoted by the IL also shifted the E" peak for lower temperatures for the optimized content of 0.4 phr. As discussed before, saturation of the filler in the resin has not been reached for this content, so the best affinity and better dispersion of AP decreases the content of resin-rich areas [8]. Moreover, the best bonding increased the capacity to dissipate energy through the interface.

Damping curves for epoxy and its AP composites are displayed in Fig. 7, and the main properties obtained from these curves are represented in Table 3. For polymeric systems, it is possible to correlate the energy absorption with the tan delta peak height, where the difference between storage and loss moduli reaches a maximum, and, therefore, the energy dissipation is higher. For the epoxy with untreated AP, it is possible to verify a decrease in peak height compared to the neat resin, which can be related to a poor interaction between fiber and matrix.

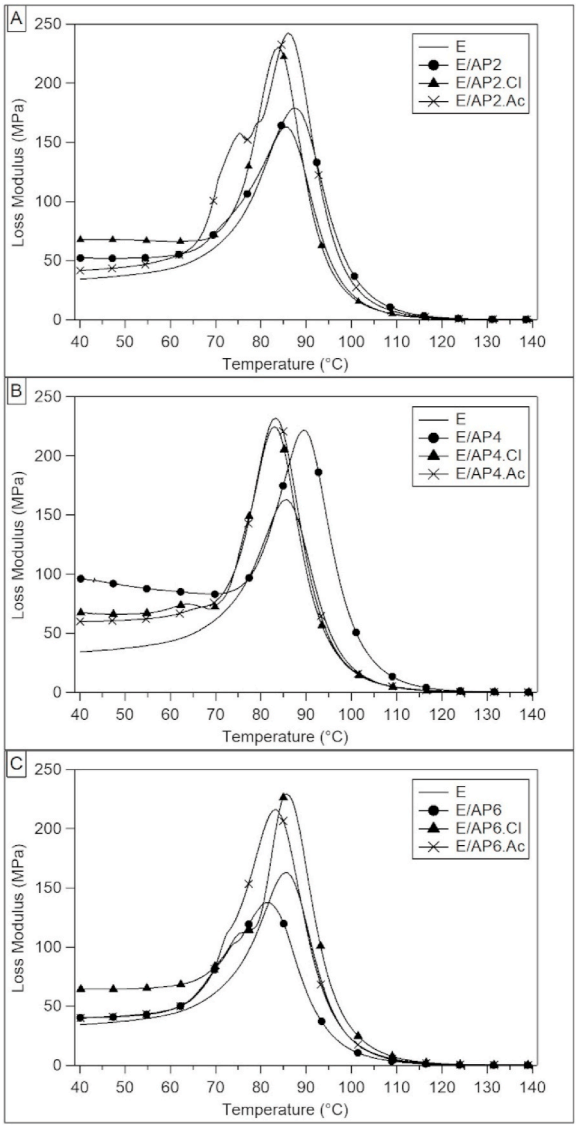

Fig. 6. Loss modulus curves for epoxy and the epoxy composites with 0.2 phr (A), 0.4 phr (B) and 0.6 phr (C) of AP.

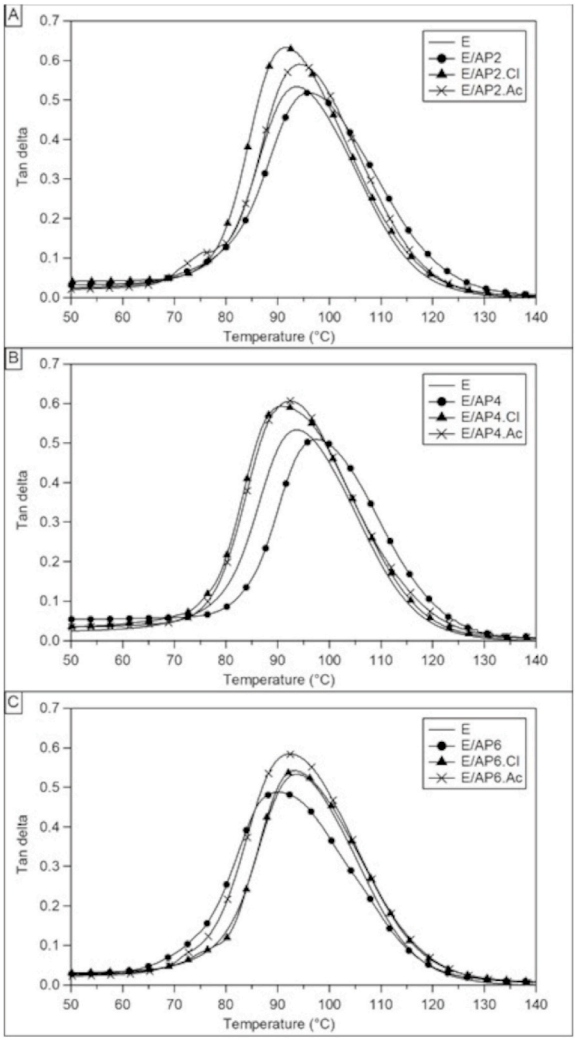

Fig. 7. Damping curves for epoxy and the epoxy composites with 0.2 phr (A), 0.4 phr (B) and 0.6 phr (C) of AP.

Table 3
Summarized values from damping curves for the epoxy/AP composites.

Sample	T_g (°C)[a]	Peak height[a]	FWHM (°C)[a]
E	93.3	0.53	22.2
E/AP2	95.9	0.52	24.4
E/AP4	97.4	0.51	22.2
E/AP6	90.0	0.49	25.8
E/AP2.Cl	91.9	0.63	22.1
E/AP4.Cl	90.7	0.59	24.2
E/AP6.Cl	93.4	0.54	22.8
E/AP2.Ac	94.1	0.59	22.6
E/AP4.Ac	92.4	0.61	23.4
E/AP6.Ac	92.7	0.58	24.7

[a] Note: T_g, glass transition temperature determined as the temperature of damping curves' peak; FWHM, full width at half-maximum values of damping curves.

Moreover, the higher the content of untreated AP, the lower the tan δ peak height, a result again related to the poor homogeneity of this system. On the other hand, when AP was treated with one of the IL there were increases of tan δ peak height, regardless the content used, highlighting those obtained with **E/AP2.Cl** and **E/AP4.Ac**.

If a stronger interfacial region is formed between the polymer matrix and AP, the T_g of the composite can increase [33]. Moreover, the shifting of the damping curves to higher temperatures indicates decreased mobility of the polymer chains from the addition of fillers and the improved interfacial adhesion [34], in this case governed by hydrogen bonds between AP-IL and cured IL-epoxy matrix. The use of AP into the composite may hinder the movement of polymer chains. Hence, the use of treated AP can combine higher T_g and stiffness, for a more crosslinked structure, and greater energy dissipation, from the increment seen in tan δ peak height. These characteristics are presented in Table 3 for those composites **E/AP2.Ac** and **E/AP6.Cl**, compared to the neat resin.

The parameter full width at half-maximum values of damping curves (FWHM) may be used to assess composite homogeneity, and the lower the value, the higher the homogeneity [8]. In this study, the FWHM values were mostly similar, which can be associated with the low reinforcement content. A Cole-Cole plot can also be used to assess composite homogeneity [34,35], where narrower curves indicate greater homogeneity [34]. When a better distribution of the filler into the polymer matrix is reached, a smaller difference in relaxation times for each composite's component (i.e., AP + epoxy) is observed, especially for the samples with higher AP content (0.6 phr). In Fig. 8 it can be seen that the use of both IL resulted in more homogeneous composites, especially for **C_4MImCl**. In this case, the stronger interaction, governed by hydrogen bonding between AP-IL and cured IL-epoxy matrix, can also improve the distribution of AP into the composite, as also discussed for storage modulus results.

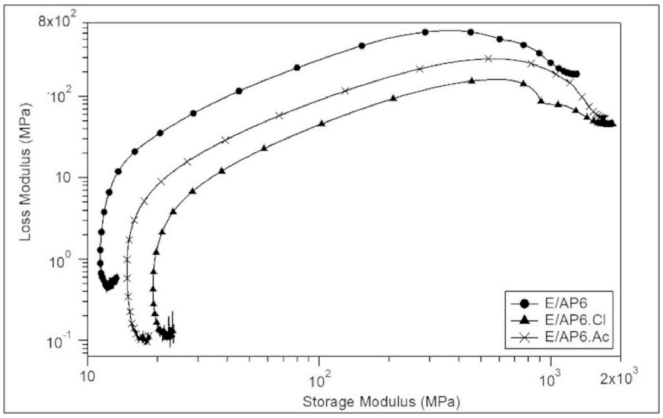

Fig. 8. Cole-Cole curves for the epoxy composites with 0.6 phr of AP.

3.2.3. *Flexural and fracture toughness behavior*

Typical curves obtained in the flexural tests are presented in Fig. S4, being similar for all samples, probably due to the low reinforcement content used. Inferential statistical analysis was applied to the flexural properties (Table 4) and showed that the use of both IL-treated AP did not promote increments for flexural modulus, related to neat epoxy, again attributed to the low content of AP. However, when compared to those with untreated AP, a significant increment is observed for E_f, regardless the IL used. This behavior is probably related to the better anchoring of the AP to the polymer through the rougher pulp surface [15,16]. Moreover, the treatment with **C_4MImCl** promoted a significant increment of 17% in flexural strength, compared to the neat polymer. Better distribution of the fillers into the composite and interfacial characteristics of the IL treated AP yielded higher load transferring between the polymer matrix and the fibers [33,36,37], which also decreased strain at break for both IL-treated AP composites. Differently, **C_4MImAc** appears to have caused a more significant damage to the pulp surface (see Fig. 4c), to the point of decreasing its mechanical properties and, in turn, of the composite. Also, its interaction with epoxy was weaker (see Fig. S2), compared with the other IL. For this reason, only the 0.2 phr content increased strength for the **E/AP.Ac**, compared to **E/AP2**.

For all samples, higher flexural moduli and strengths were obtained for 0.4 phr. Above that, there was greater AP-to-AP contact, which perhaps decreased the hydrogen bond formation between AP-IL and IL-cured epoxy. This phenomenon decreases the stress transference through the interface [38], even when the IL treatment was used.

Inferential statistical analysis was applied to the toughness properties and are shown in Table 5. For K_{IC}, there was a significant decrease for the **E/AP.Cl** composites. As presented by the NMR study (Fig. S1) and discussed in Fonseca et al. [7], the use of **C_4MImCl** can decrease the crosslink density if the system is cured at room temperature, by reducing the reactivity of the hardener through hydrogen bonding. It also explains the lower flexural strain obtained by the compositions of AP treated with this IL, and consequently, the lower K_{IC}. Moreover, a correlation between K_{IC} and flexural modulus (see Table 4) can be found, as fewer rigid materials tend to exhibit higher toughness, which is more pronounced for the **E/AP** composites.

There were no differences for both K_{IC} and G_{IC} when a higher content of AP was used, which can be related to the low filler content. However, significant decreases were observed for G_{IC} when untreated-AP and contents above 0.2 phr were used, compared to neat epoxy. According Vu et al. [5], increased toughness of epoxy based composites can be attributed to the presence of obstacles (i.e., fiber bridging), which move the crack orientation and growth. However, this effect is only observed when the reinforcement presents good anchoring by the matrix, which also changes the failure pattern, as discussed above.

Fig. 9 presents the SEM images of the cracked samples surfaces from

Table 4
Inferential statistics for the flexural results of epoxy and its composites.

Sample	E_f (MPa)[a]	σ_f (MPa)[a]	Strain at break (%)[a]
E	$1056^{8.7}$ AB	$95.3^{2.7}$ AB	$23.2^{10.3}$ B
E/AP	$929^{9.5}$ A	$91.3^{10.9}$ A	$20.4^{14.8}$ AB
E/AP.Cl	$1098^{13.7}$ B	$111.4^{9.3}$ C	$18.8^{18.2}$ A
E/AP.Ac	$1052^{13.6}$ B	$104.6^{11.8}$ BC	$20.8^{13.1}$ AB
F	4.99	9.96	2.79
Reinforcement content (phr)			
0	$1056^{8.7}$ AB	$95.3^{2.7}$ AB	$23.2^{10.3}$ B
0.2	$1030^{13.0}$ AB	$100.9^{17.2}$ AB	$20.3^{12.4}$ AB
0.4	$1064^{13.9}$ B	$107.2^{10.8}$ B	$19.3^{16.0}$ A
0.6	$967^{13.1}$ A	$96.1^{14.4}$ A	$20.2^{19.3}$ AB
F	1.52	1.96	1.73

[a] Note: values in superscript are the coefficient of variance; different uppercase letters represent statistical differences between means for that property; F = test statistic.

Table 5
Inferential statistical analysis for the fracture toughness (K_{IC}) and strain energy release rate (G_{IC}) of the epoxy/AP composites.

Sample	K_{IC} (MPa.m^{-2})[a]	G_{IC} (kJ.m^{-2})[a]
E	$1.58^{5.0}$ AB	$3.07^{4.9}$ B
E/AP	$1.57^{9.3}$ B	$2.61^{4.06}$ A
E/AP.Cl	$1.31^{12.6}$ A	$2.78^{5.8}$ AB
E/AP.Ac	$1.50^{20.5}$ AB	$2.79^{14.5}$ AB
F	2.61	3.53
Reinforcement content (phr)		
0	$1.58^{5.0}$ A	$3.07^{4.9}$ B
0.2	$1.42^{9.7}$ A	$2.78^{7.8}$ AB
0.4	$1.52^{20.9}$ A	$2.74^{8.2}$ A
0.6	$1.51^{16.9}$ A	$2.59^{13.0}$ A
F	1.52	3.12

[a] Note: values in superscript are the coefficient of variance; different uppercase letters represent statistical differences between means for that property; F = test statistic.

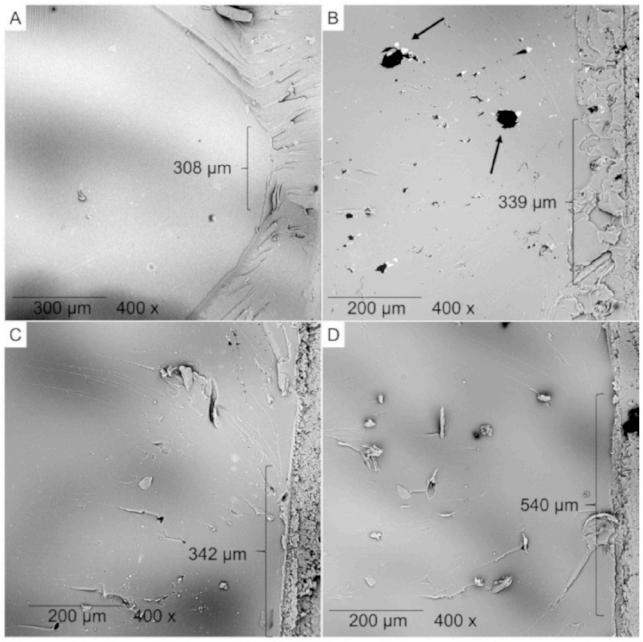

Fig. 9. SEM micrographs of the crack's initiation on the surface for neat epoxy (A), **E/AP4** (B), **E/AP4.Ac** (C) and **E/AP4.Cl** (D).

SENB tests. The incorporation of AP increased the zone of plastic deformation (ZPD), especially when the AP was treated with IL. According to Fonseca et al. [7], a larger ZPD indicates greater capacity to absorb energy by plastic deformation, which is related to the improved bonding between IL-treated AP and cured epoxy. Moreover, the composites presented a rougher fracture surface, compared to the neat resin (Fig. 9a). This also suggests higher energy absorption during crack growth when the load was applied [5,6]. Finally, **E/AP4** presented some fiber pull-out, indicated by arrows in Fig. 9b, related to the poor adhesion of the AP to the epoxy matrix, which can be partly responsible for the lower G_{IC} value. In that case, the energy required for fiber pull-out was lower than that for fiber break, this later behavior observed for the composites with IL-treated AP (Fig. 9c–d).

4. Conclusions

The surface treatment and modification of AP using two types of physiosorbed IL, **C_4MImCl** and **C_4MImAc**, was successfully reported. Moreover, epoxy-based composites with different ratios of IL-treated AP were obtained using a simplified methodology, compared to those of current literature. Both IL represent a good alternative as aramid fibers surface modifiers, promoting fibrillation. These morphological features promoted greater anchoring of the epoxy matrix to the AP. Moreover, both IL promoted the formation of hydrogen bonds between the hardener and the AP, which can also increase the affinity with the cured epoxy matrix. These morphological and chemical differences were mostly responsible for the differences found in the mechanical and viscoelastic characteristics of the composites, highlighting the ability of **C_4MImCl** to form stronger hydrogen bonds with the cured epoxy. For those AP treated with **C_4MImAc**, toughening of the epoxy was achieved, which was credited to the presence of the fibrillated reinforcement and, consequently, the greater anchoring of the filler by the polymer.

Funding

This work was financed by Coordination for the Improvement of Higher-Level Education (CAPES) and the National Council for Scientific and Technological Development (CNPq).

Availability of data and material

The authors declare that all data used are available upon request.

Code availability

The authors declare that all code or software used are available.

Authors' contributions

Eduardo Fischer Kerche: conceptualization, methodology, formal analysis, writing- original draft. Vinícius Demétrio da Silva: conceptualization, methodology, investigation, writing. Eduardo Fonseca: conceptualization, methodology, samples characterization, results analysis, writing. Nicholas Salles: Samples' preparation and methodology. Henri Stephan Schrekker: review, editing and supervision. Sandro Campos Amico: review, editing, supervision and project administration.

Declaration of competing interest

The authors declare that they have no known competing financial interests or personal relationships that could have appeared to influence the work reported in this paper.

Acknowledgments

This study was partly financed by the Coordenação de Aperfeiçoamento de Pessoal de Nivel Superior – Brasil (CAPES), Finance Code 001, and especially the CAPES/STINT project. The authors thank CNPq for the partial financial support. DuPont is kindly acknowledged for the donation of the aramid pulp.

Appendix A. Supplementary data

Supplementary data to this article can be found online at https://doi.org/10.1016/j.polymer.2021.123787.

References

[1] P. Dittanet, R.A. Pearson, Effect of silica nanoparticle size on toughening mechanisms of filled epoxy, Polymer 53 (2012) 1890–1905, https://doi.org/10.1016/j.polymer.2012.02.052.
[2] D.A. Norman, R.E. Robertson, Rigid-particle toughening of glassy polymers, Polymer 44 (2003) 2351–2362, https://doi.org/10.1016/S0032-3861(03)00084-3.
[3] D. Incerti, T. Wang, D. Carolan, A. Fergusson, Curing rate effects on the toughness of epoxy polymers, Polymer 159 (2018) 116–123, https://doi.org/10.1016/j.polymer.2018.11.008.
[4] K.P. Unnikrishnan, E.T. Thachil, Toughening of epoxy resins, Des. Monomers Polym. 9 (2006) 129–152, https://doi.org/10.1163/156855506776382664.

[5] C.M. Vu, L.H. Sinh, D.D. Nguyen, H.V. Thi, H.J. Choi, Simultaneous improvement of the fracture toughness and mechanical characteristics of amine-functionalized nano/micro glass fibril-reinforced epoxy resin, Polym. Test. 71 (2018) 200–208, https://doi.org/10.1016/j.polymertesting.2018.09.005.
[6] H. Ma, M.A. Aravand, B.G. Falzon, Synergistic enhancement of fracture toughness in multiphase epoxy matrices modified by thermoplastic and carbon nanotubes, Compos. Sci. Technol. 201 (2021) 108523, https://doi.org/10.1016/j.compscitech.2020.108523.
[7] E. Fonseca, V. Demétrio da Silva, J.S. Klitzke, H.S. Schrekker, S.C. Amico, Imidazolium ionic liquids as fracture toughening agents in DGEBA-TETA epoxy resin, Polym. Test. 87 (2020) 106556, https://doi.org/10.1016/j.polymertesting.2020.106556.
[8] H.L. Ornaghi, A.S. Bolner, R. Fiorio, A.J. Zattera, S.C. Amico, Mechanical and dynamic mechanical analysis of hybrid composites molded by resin transfer molding, J. Appl. Polym. Sci. 118 (2010) 887–896, https://doi.org/10.1002/app.32388.
[9] P.K. Mallick, Fibre-reinforced Composites Materials, Manufacturing and Design, third ed., CRC Press, New York, 2007 https://doi.org/10.1016/0010-4361(89)90651-4.
[10] S.N. Raja, S. Basu, A.M. Limaye, T.J. Anderson, C.M. Hyland, L. Lin, A.P. Alivisatos, R.O. Ritchie, Strain-dependent dynamic mechanical properties of Kevlar to failure : structural correlations and comparisons to other polymers, Mater. Today Commun. 2 (2015) e33–e37, https://doi.org/10.1016/j.mtcomm.2014.11.002.
[11] J. Wu, X.H. Cheng, Effect of surface treatment on the mechanical and tribological performance of Kevlar pulp reinforced epoxy composites, Tribol. Lett. 24 (2006) 195–199, https://doi.org/10.1007/s11249-006-9138-0.
[12] Y. Hu, F. Cheng, Y. Ji, B. Yuan, X. Hu, Effect of aramid pulp on low temperature flexural properties of carbon fibre reinforced plastics, Compos. Sci. Technol. 192 (2020) 108095, https://doi.org/10.1016/j.compscitech.2020.108095.
[13] J. Nasser, L. Zhang, H. Sodano, Aramid nanofiber interlayer for improved interlaminar properties of carbon fiber/epoxy composites, Compos. Part B. 197 (2020) 108130, https://doi.org/10.1016/j.compositesb.2020.108130.
[14] B. Zhang, L. Jia, M. Tian, N. Ning, L. Zhang, W. Wang, Surface and interface modification of aramid fiber and its reinforcement for polymer composites: a review, Eur. Polym. J. 147 (2021) 110352, https://doi.org/10.1016/j.eurpolymj.2021.110352.
[15] V.D. da Silva, M.M. Jacobi, H.S. Schrekker, S.C. Amico, Aramid pulp with physisorbed imidazolium ionic liquids for solvent-casted enhanced styrene-butadiene rubber composites, J. Appl. Polym. Sci. 135 (2018) 46693, https://doi.org/10.1002/app.46693.
[16] V.D. da Silva, M.M. Jacobi, H.S. Schrekker, S.C. Amico, Imidazolium ionic liquid compatibilizers in melt - blended styrene - butadiene rubber/aramid pulp composites, Polym. Bull. 76 (2019) 3451–3462, https://doi.org/10.1007/s00289-018-2550-4.
[17] V.D. da Silva, Í.R. de Barros, D.K.S. da Conceição, K.N. de Almeida, H.S. Schrekker, S.C. Amico, M.M. Jacobi, Aramid pulp reinforced hydrogenated nitrile butadiene rubber composites with ionic liquid compatibilizers, J. Appl. Polym. Sci. 137 (2020) 48702, https://doi.org/10.1002/app.48702.
[18] C.V. Moraes, V.D. da Silva, M.V. Castegnaro, J. Morais, H.S. Schrekker, S.C. Amico, Lightweight composites through imidazolium ionic liquid enhanced aramid – epoxy resin interactions, ACS Appl. Polym. Mater. 2 (2020) 1754–1763, https://doi.org/10.1021/acsapm.9b01145.
[19] E.F. Kerche, V. Demétrio da Silva, G. da S. Jankee, H.S. Schrekker, R. de A. Delucis, Aramid pulp treated with imidazolium ionic liquids as a filler in rigid polyurethane bio-foams, J. Appl. Polym. Sci. 138 (2021) 50492, https://doi.org/10.1002/app.50492.
[20] S. Dewilde, J. Winters, W. Dehaen, K. Binnemans, Polymerization of PPTA in ionic liquid/cosolvent mixtures, Macromolecules 50 (2017) 3089–3100, https://doi.org/10.1021/acs.macromol.7b00579.
[21] S. Dewilde, T. Vander Hoogerstraete, W. Dehaen, K. Binnemans, Synthesis of poly-p-phenylene terephthalamide (PPTA) in ionic liquids, ACS Sustain. Chem. Eng. 6 (2018) 1362–1369, https://doi.org/10.1021/acssuschemeng.7b03727.
[22] Dupont, Kevlar® Aramid Pulp, (n.d.). https://www.dupont.com/products/dupont-kevlar-aramid-pulp.html (accessed March 1, 2021).
[23] S. Villar-Rodil, J.I. Paredes, A. Martinez-Alonso, J.M.D. Tascón, Atomic force microscopy and infrared spectroscopy studies of the thermal degradation of Nomex aramid fibers, Chem. Mater. 13 (2001) 4297–4304, https://doi.org/10.1021/cm001219f.
[24] S.A. Dharaskar, M.N. Varma, D.Z. Shende, C.K. Yoo, K.L. Wasewar, Synthesis, characterization and application of 1-butyl-3 methylimidazolium chloride as green material for extractive desulfurization of liquid fuel, Sci. World J. 2013 (2013) 1–9, https://doi.org/10.1155/2013/395274.
[25] M.L. Williams, S.P. Holahan, M.E. McCorkill, J.S. Dickmann, E. Kiran, Thermal and spectral characterization and stability of mixtures of ionic liquids [EMIM]Ac and [BMIM]Ac with ethanol, methanol, and water at ambient conditions and at elevated temperatures and pressures, Thermochim. Acta 669 (2018) 126–139, https://doi.org/10.1016/j.tca.2018.09.013.
[26] J.S. Lin, Effect of surface modification by bromination and metalation on Kevlar fibre-epoxy adhesion, Eur. Polym. J. 38 (2002) 79–86, https://doi.org/10.1016/S0014-3057(01)00176-8.
[27] S. Li, K. Han, H. Rong, X. Li, M. Yu, Surface modification of aramid fibers via ammonia-plasma treatment, J. Appl. Polym. Sci. 131 (2014), https://doi.org/10.1002/app.40250 n/a-n/a.
[28] M.N.C. Zarycz, C. Fonseca Guerra, NMR 1H-Shielding constants of hydrogen-bond donor reflect manifestation of the pauli principle, J. Phys. Chem. Lett. 9 (2018) 3720–3724, https://doi.org/10.1021/acs.jpclett.8b01502.
[29] M.G. Siskos, A.G. Tzakos, I.P. Gerothanassis, Accurate ab initio calculations of O-H···O and O-H···O proton chemical shifts: towards elucidation of the nature of the hydrogen bond and prediction of hydrogen bond distances, Org. Biomol. Chem. 13 (2015) 8852–8868, https://doi.org/10.1039/c5ob00920k.
[30] J.D. McCoy, W.B. Ancipink, C.M. Clarkson, J.M. Kropka, M.C. Celina, N.H. Giron, L. Hailesilassie, N. Fredj, Cure mechanisms of diglycidyl ether of bisphenol A (DGEBA) epoxy with diethanolamine, Polymer 105 (2016) 243–254, https://doi.org/10.1016/j.polymer.2016.10.028.
[31] R.M. Neves, A.B. Vanzetto, L.K. Lazzari, A.J. Zattera, Thermal and dynamic mechanical behavior of epoxy composites reinforced with post-consumed yerba mate, J. Appl. Polym. Sci. 138 (2021) 50438, https://doi.org/10.1002/app.50438.
[32] A. Lavoratti, A.J. Zattera, S.C. Amico, Mechanical and dynamic-mechanical properties of silane-treated graphite nanoplatelet/epoxy composites, J. Appl. Polym. Sci. 135 (2018) 46724, https://doi.org/10.1002/app.46724.
[33] J. Jung, H.A. Sodano, High strength epoxy nanocomposites reinforced by epoxy functionalized aramid nanofibers, Polymer 195 (2020) 122438, https://doi.org/10.1016/j.polymer.2020.122438.
[34] J.H.S. Almeida Júnior, H.L. Ornaghi Júnior, S.C. Amico, F.D.R. Amado, Study of hybrid intralaminate curaua/glass composites, Mater. Des. 42 (2012) 111–117, https://doi.org/10.1016/j.matdes.2012.05.044.
[35] L.A. Pothan, Z. Oommen, S. Thomas, Dynamic mechanical analysis of banana fiber reinforced polyester composites, Compos. Sci. Technol. 63 (2003) 283–293, https://doi.org/10.1016/S0266-3538(02)00254-3.
[36] C. Chen, J. Liu, X. Li, Y. Wen, X. Li, D. Shi, Z. Xue, Epoxy/ionic liquid-like MWCNTs composites with improved processability and mechanical properties, Compos. Commun. 15 (2019) 46–52, https://doi.org/10.1016/j.coco.2019.06.001.
[37] J. Wang, Z. Chen, A. Qi, N. Raymonde, H.E. Naguib, Ionic liquids facilitated dispersion of chitin nanowhiskers for reinforced epoxy composites, Carbohydr. Polym. 247 (2020) 116746, https://doi.org/10.1016/j.carbpol.2020.116746.
[38] A. Watters, J. Cuadra, A. Kontsos, G. Palmese, Processing-structure – property relationships of SWNT – epoxy composites prepared using ionic liquids, Compos. Part A. 73 (2015) 269–276, https://doi.org/10.1016/j.compositesa.2015.03.019.